Available online at www.sciencedirect.com

ScienceDirect

www.elsevier.com/locate/matchar

Layered-structural monoclinic–orthorhombic perovskite $La_2Ti_2O_7$ to orthorhombic $LaTiO_3$ phase transition and their microstructure characterization

G. Herrera[a,b,c,*], J. Jiménez-Mier[c], E. Chavira[d]

[a]Colegio de Física, ENP P7, "Ezequiel A. Chávez", Universidad Nacional Autónoma de 3México, 15810 México D. F., Mexico
[b]Departamento de Química Inorgánica, Universidad de Valencia, 46100 Burjasot, Valencia, Spain
[c]Instituto de Ciencias Nucleares, Universidad Nacional Autónoma de México, 04510 México D. F., Mexico
[d]Instituto de Investigaciones en Materiales, Universidad Nacional Autónoma de México, 04510 México D. F., Mexico

ARTICLE DATA

Article history:
Received 23 May 2013
Received in revised
form 23 December 2013
Accepted 24 December 2013

Keywords:
X-ray diffraction
Scanning electron microscopy
Ceramics

ABSTRACT

The layered-structural ceramics, such as lanthanum titanate ($La_2Ti_2O_7$), have been known for their good temperature and low dielectric loss at microwave frequencies that make them good candidate materials for high frequency applications. However, few studies have been conducted on the synthesis optimization by sol gel reaction, in particular by acrylamide polymerization route. The interest in $La_2Ti_2O_7$ ceramic has been greatly increased recently due to the effect of oriented grains. This anisotropy of the microstructure leads to anisotropy in dielectric, electrical and mechanical properties. In this study, grain oriented lanthanum titanate was produced by the sol–gel acrylamide polymerization route. The characterizations of the samples were achieved by thermal analysis, X-ray diffraction (XRD), scanning electron microscopy (SEM), atomic force microscopy (AFM), and transmission electron microscopy (TEM). X-ray diffraction indicates that the formation of monoclinic perovskite $La_2Ti_2O_7$ nanocrystals is a necessary first step to obtain orthorhombic $LaTiO_3$ nanocomposites (with space group Pbnm). In this work we identified that the monoclinic perovskite $La_2Ti_2O_7$ with space group $P2_1$ transforms its structure into one with the orthorhombic space group $Cmc2_1$ at approximately 1073 K. The microstructure associated consisted of flaky monoclinic $La_2Ti_2O_7$ nanocomposites in comparison with round-shaped $LaTiO_3$ nanocomposites.

1. Introduction

The largest number of perovskite-type compounds is described by the general formula ABO_3 [1]. About 50 years ago, Aurivillius discovered a family of layered structural ceramic materials [2]. Lanthanum titanate, $La_2Ti_2O_7$, is a member of the perovskite layer structure (PLS) family of ferroelectrics sometimes referred to as the strontium pyroniobate family [3,4]. The structure of PLS compounds is characterized by perovskite slabs stacked along the *a* axis, which are made up of corner-sharing BO_6 octahedra and 12 coordinated A cations. Each slab is four octahedra thick and is linked to a neighboring slab by A cations lying near the boundary [5,6]. In other words the $A_2B_2O_7$ structure has an extra layer of O_2 inserted along the

* *Corresponding author at: Colegio de Física, ENP P7 "Ezequiel A.* Chávez", Universidad Nacional Autónoma de México, Calz. de la Viga # 54, Merced Balbuena, Venustiano Carranza, 15810, Mexico City, Mexico. Tel.: +52 55 57 72 44 76.
E-mail addresses: manuel.herrera@enp.unam.mx, guillermo.m.herrera@uv.es (G. Herrera).

1044-5803/$ – see front matter © 2013 Elsevier Inc. All rights reserved.
http://dx.doi.org/10.1016/j.matchar.2013.12.013

perovskite [110] direction after every four (n) distorted perovskite units [7]. The anisotropy of the structure leads to anisotropy in dielectric, electrical and mechanical properties [8].

$La_2Ti_2O_7$ do not form the expected isometric pyrochlore structure-type. The stability of this structure depends on the ratio between the cations radii of Ln^{3+} and Ti^{4+}. For r (Ln^{3+})/r (Ti^{4+}) included in the range [1.46–1.78], the formed compound will adopt a pyrochlore like structure. For a ratio higher than 1.78, the layered perovskite type is preferred. Finally for a ratio lower than 1.46, the formed compound will favor a defect fluorite structure [9]. According to the ratio r (Ln^{3+})/r (Ti^{4+}) = 1.92 obtained using the ionic radii from Shannon [10], the $La_2Ti_2O_7$ compound studied in this work crystallizes in a monoclinic perovskite layered structure with a $P2_1$ space group. The measured unit cell parameters of monoclinic $La_2Ti_2O_7$, the number of molecules per unit cell (Z), and the theoretical density (ρ) are a = 7.8114(2), b = 5.5474(1), c = 13.0185(1) Å, β = 98.719°, Z = 4, and ρ = 5.78 g cm^{-3}, respectively [11].

Ishizawa et al. [6] have shown that the structure changes from monoclinic ($P2_1$) to orthorhombic phase ($CmC2_1$) at temperatures higher than 1053 K in which spontaneous polarization appears along the b axis due to an asymmetric deformation of the TiO_6 octahedra (Fig. 1). In the temperature range of 1053–993 K, there is another ferroelectric–ferroelectric phase change from orthorhombic to monoclinic, $P2_1$ [6,7]. This transition is characterized by a rotation that occurs through the Ti^{4+} ions without deforming the shapes of the octahedra, resulting in a small change in magnitude of the dipole moment in each respective TiO_6 octahedron [6]. Above 1773 K, the structure undergoes further transformation into the para-electric phase (Cmcm) [6].

$La_2Ti_2O_7$ has been synthesized previously using different techniques; solid state processing [3], co-precipitation of hydroxides [12,13], urea precipitation [14], hydrothermal synthesis [15,16] the high-temperature decomposition of metal-organic precursors [17,18], thermal decomposition of nitrates [19], and liquid mix techniques [20]. These syntheses not only have provided for smaller particle sizes compared to the solid-state method, but also typically require extended heating times and multi-step synthetic procedures. It has also been synthesized in the form of thin films using molecular beam epitaxy (MBE) [21,22], pulsed laser deposition (PLD) [23,24] and laser heated pedestal growth [25].

In recent years, the sol–gel process has become a method of interest for the synthesis of nano-composites and electroceramics [26–31]. The advantages of the sol–gel process compared to conventional methods for polycrystalline ceramics are better control of stoichiometry and homogeneity, lower reaction temperatures, less contamination, and ease of preparation of ultrafine powders, thin films, and fibers for device applications. By adjusting firing temperatures, it should be possible to control the degree of crystallization and grain sizes. Sol–gel processing is very cost effective compared to techniques such as chemical vapor deposition, sputtering, and laser ablation because it does not require expensive vacuum equipment or raw materials. Our research efforts in this area have focused on the optimization of synthesis steps of metal-oxides to produce homogeneous grain size and shape distribution [32–37].

Furthermore lanthanum titanate is an effective ferroelectric substance. This compound has a high Curie temperature (Tc = 1773 K), which is particularly interesting for high-temperature piezoelectric applications [25,38]. Consequently, it can be used in ferroelectric random access memory [39] and ferroelectric gate field-effect transistors [40].

Its temperature stability and low dielectric loss (with dielectric constant in the range ε_r = 42–62) at microwave frequencies make it good candidate materials for high frequency applications, high temperature transducer material [25] and electro optic devices [28,41,42]. It can conveniently be used above 1273 K for controlling intelligent gas turbine engines. It is also under consideration as low temperature coefficient of capacitance (TCC) materials [43,44]. It has low spontaneous polarization: Ps = 5 mC/cm^2 with the polarization oriented along the b-axis (polar axis) [11]; high coercive field (45 kV/cm) [11,38] and high remanent polarization. Furthermore, it has been reported that $La_2Ti_2O_7$ oxides can act as excellent hosts for integration by substitution of lanthanide ions to produce phosphors emitting a variety of colors for the development of photoluminescent materials [45,46].

$La_2Ti_2O_7$ is a highly donor-doped layered perovskite structure which has photocatalytic applications, including water-splitting under visible light irradiation and UV irradiation [29,47], Cr(VI) reduction [48], NO oxidation [49], for producing hydrogen from water photosplitting and photodegradation of organic pollutants [14,18,50–52] It has a great ability for the realization of immobilization matrices of highly active radio-nuclides from nuclear wastes [53]. It is especially useful for treating waste water containing traces of toxic organic substances. The separation of electrons and holes in the perovskites is easier than that in other semiconductor materials because of their narrower depletion layers. The reported quantum yields of the (1 1 0) layered perovskites range as high as ~20–50% at ultraviolet wavelengths [53,54]. This result is much higher than that (<1%) of TiO_2. Abe et al. [55] reported that the high photocatalytic water-splitting activity of these perovskite structured catalysts could be attributed to their octahedral structure to enhance the mobility of photogenerated electrons and holes.

The orthorhombic $LaTiO_3$, on the other hand, at room temperature possesses the orthorhombic $GdFeO_3$ perovskite structure (space group Pbnm No. 62) with lattice parameters: a = 5.604 Å, b = 5.595 Å, and c = 7.906 Å [56,57]. It is considered a Mott insulator with a G-type antiferromagnetic ordered ground state and a Néel temperature of approximately 135 K. $LaTiO_3$ is a semiconductor at high temperature, becoming an antiferromagnetic insulator upon cooling through the Néel temperature. When synthesized with moderate oxygen content, $LaTiO_{3+x}$ is metallic at high temperature, with a metal-insulator transition occurring at reduced temperature. Transport measurements on bulk samples indicate that $LaTiO_{3.4}$ is a p-type semiconductor [58]. The effect of Sr doping on $LaTiO_3$ is being considered for numerous applications, including conducting electrodes for ferroelectrics [59] and dielectric-base transistors [60], as well as for sensors [61].

The objectives of this work are to investigate (i) the phase stability of monoclinic perovskite $La_2Ti_2O_7$ and orthorhombic perovskite $La_2Ti_2O_7$ crystal structures by decreasing the thermal treatment of the amorphous powders prepared by sol–gel acrylamide polymerization route. Also, the phase stability evaluation of the orthorhombic perovskite $LaTiO_3$; (ii) the effects of heat treatments on the microstructure of

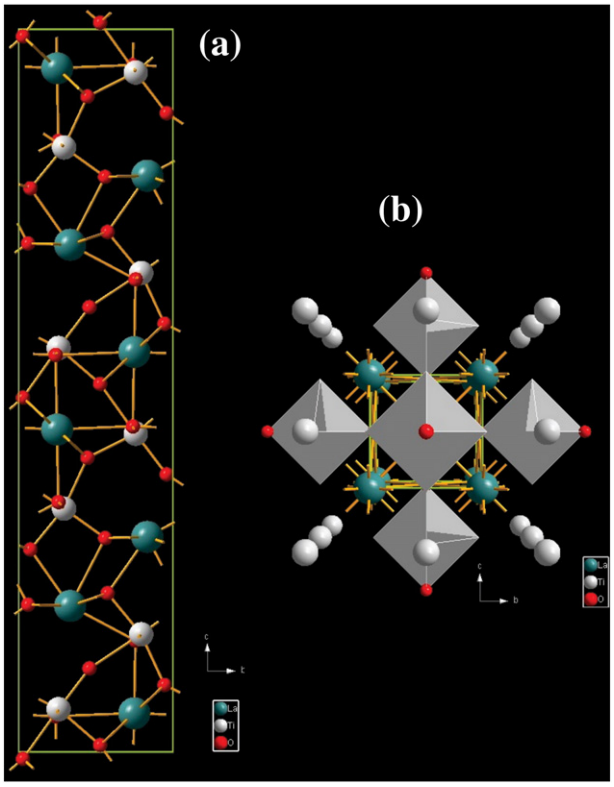

Fig. 1 – (a) Schematic representation of the Cmc2$_1$ phase of $La_2Ti_2O_7$ studied in this work. The small (red), medium (gray), and big (green) balls represent O, Ti, and La atoms, respectively. (b) Schematic representation of the Pbnm phase of $LaTiO_3$. These structures were obtained by Diamond 3.2 software.

monoclinic–orthorhombic $La_2Ti_2O_7$ up to orthorhombic $LaTiO_3$ compounds. The characterization tools used in this work are: thermal analysis: (differential thermal analysis DTA, thermo gravimetric TG and differential scanning calorimetry DSC); X-ray diffraction (XRD); scanning electron microscopy (SEM); energy dispersive X-rays (SEM/EDX), atomic force microscopy (AFM) and transmission electron microscopy (TEM).

2. Experimental Procedure

2.1. Sol–gel Acrylamide Synthesis, SGAP

2.1.1. Materials

La_2O_3 (CERAC, 99.99%) and TiO_2 (CERAC, 99.9%); HNO_3 (J.T. Baker, 69–70%); ethylenediamine tetraacetic acid, EDTA [CH2N(CH2CO2H)2]2 (Fluka, 99%); NH_4OH (J.T. Baker, 28–30%); acrylamide, $H_2C = CHCONH_2$ (Fluka, 99.9%); N, N′-methylene bisacrylamide, $C_7H_{10}N_2O_2$ (Fluka, 99.5%) and α, α′-azodiisobutyramidine dihydrochloride, AIBN, $C_8H_{18}N_6 \cdot 2HCl$ (Fluka, 98%) were used in the fabrication of $La_2Ti_2O_7$ by SGAP. The flow diagram for this SGAP route is shown in Fig. 2.

2.1.2. Sol Formation

In order to obtain 2 g of the sample, a 50 mol% of stoichiometric proportion of La_2O_3 compound was dissolved in 150 ml of distilled water slowly with 4 ml of HCl (Sigma-Aldrich, 36.5–38.0%) to obtain a transparent solution. 50 mol% of TiO_2 was putted in 25 ml of distilled water. A suspension formation of TiO_2 was observed after we have added slowly 25 ml of H_2SO_4 (Sigma-Aldrich, 95.0–98.0%). In this step and in order to avoid a precipitation of this suspension, the temperature at 50 °C was kept in the magnetic stirrer (Ika CERAMAG model Mid) during 30 min.

2.1.3. Gel Formation

Each sol was mixed with the chelating agent, EDTA, using the molar ratio (M:EDTA 1:1), where M is the metal in the sol. EDTA combines with metal ions to form stable chelates, in a 1:1 ratio regardless of the charge on the cation [35,36,62]. We used this chelating agent to encapsulate the rare earth element La (3+) and the transition element Ti (4+) metal ions. The mixture was kept at 25 °C under constant stirring. This step was designed to prevent the ions from forming complexes until the "in situ" reactions start. The ions then keep their stability during the decomposition of EDTA.

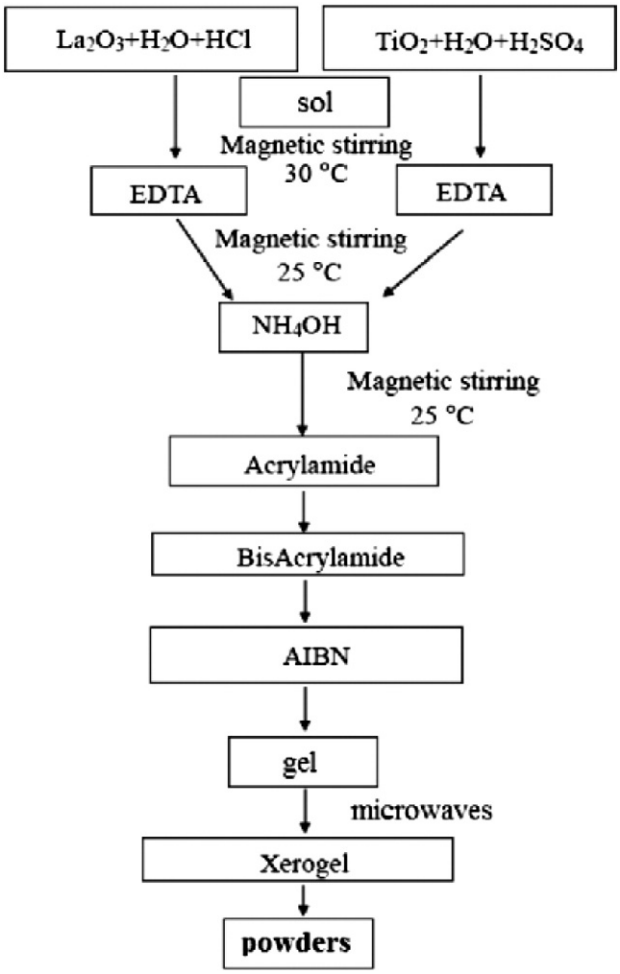

Fig. 2 – Flow chart of the sol–gel acrylamide polymerization route for the La–Ti precursor.

After this step the pH value was 0.56. The solution was then mixed, with 10–20 ml of NH_4OH in order to adjust the pH to 6 because the fast acrylamide polymerization generally proceeds in aqueous medium whose pH is close to neutral [63]. This process was performed at room temperature. To the solution (300 ml) we added a 10 wt.% of $H_2C{=}CHCONH_2$ monomers to start the polymerization [63] and to accelerate the gel formation. We added 2 wt.% of the cross-linker, $C_7H_{10}N_2O_2$. Also 1 wt.% of $C_8H_{18}N_6{\cdot}2HCl$ was added to regulate the weight of acrylamide and to increase the velocity of interconnections. The thermo-polymerization process was carried out under continuous magnetic stirring at 80 °C for 2 min until an opaque yellow viscous gel is produced.

2.1.4. Xerogel Formation

We obtained the desiccate gel (xerogel) under an Ar atmosphere using a microwave oven (SEV-MIC IV) operating at 600 W for 30 min. This xerogel was grinded in an agate RM 100 mortar (Retsch), and the powder was heated first to 100 °C during 12 h. Next we increased the temperature in 100 °C steps up to 600 °C in a thermolyne 46100 furnace maintaining the temperature during 12 h in each step. In this stage important organic and amorphous materials are removed and nanocrystals are grown as we will discuss in the DTA and XRD sections. The temperature was increased at a rate of 5 °C/min. At the end of the synthesis we obtained 96% (1.92 g) of the sample. The mixture was then compacted into pellets (diameter 13 mm thickness 1.0–1.5 ± 0.05 mm) exerting a pressure of 4 t/cm^2 in a Press (Osyma) for 3 min under vacuum.

2.2. Reduction of Samples

The pure phase of $La_2Ti_2O_7$ powders prepared by sol–gel route was compacted into pellets and then reduced with a metallic Ti rod (Aldrich 99%). Each sample and a metallic Ti rod were enclosed in a quartz tube in vacuum. The temperature was kept at 850 °C during 5 days. After this period of time the sample was quenched in ice. In this step one can observe the oxidation of metallic Ti rod.

2.3. Characterization Techniques

In order to determine the temperature interval in which the reaction should be carried out thermo gravimetric analysis (TGA) was performed using Hi-Res 2950 TGA (TA Instruments). The differential thermal (DTA) measurement was obtained in a 2910 DTA with DTA 1600 cell (TA instruments). TGA was used to evaluate the thermal decomposition of the samples prepared by SGAP. DTA and differential scanning calorimetry (DSC) were used to follow the thermal transformations such as decomposition, phase transformation, chemical stability, and volatilization of organic material of samples. The xerogel obtained by SGAP was placed in platinum crucibles and heated starting at room temperature and up to 1000 °C. The heating rates to obtain DTA and TGA were 10 °C/min under a N_2 atmosphere. The DTA and DSC curves were analyzed by universal analysis software [64].

Crystalline phases were identified by XRD, using a Bruker-AXS D8-Advance with Vantec-1 detector diffractometer with λ (CuK) = 1.5406 Å radiation. This equipment is able to detect up to a minimum of 1% of impurities. Diffraction patterns were collected at room temperature in a 10–70° range with a step size of 0.02° and time per step of 10 s. Lattice constants and other structural parameters of both $La_2Ti_2O_7$ and $LaTiO_3$ phases were determined by refinement with the Rietveld technique using Fullprof98 [65,66] available in the software package Winplotr [67]. The refinement involved the following parameters: scale factor; zero displacement correction; unit cell parameters; peak profile parameters using a pseudo-Voight function; and overall temperature factor.

The change in morphology was investigated by scanning electron microscopy, SEM, on a Cambridge-Leica Stereoscan 400. The micrographs were taken between 5 kX and 20 kX with a voltage of 20 kV, current intensity of 1000 pA and a work distance of 25 mm. The EDX was performed on the same equipment, with an Oxford/Link System electron probe microanalyzer (EPMA).

An atom force microscope AFM (JSPM-4210) equipped with tip NSC151SI3N4 with a nominal radii <10 nm, a cantilever strength constant of 40 N/m and frequency constant of 325 kHz in tapping mode was used to investigate the surface morphology, particle size and porosity. The particle size distribution and the roughness were measured by means of AFM according to three parameters: the standard deviation of the Z ranges (RMS), the arithmetic average of the absolute values of the surface height deviations measured from the mean plane (Ra) and peak-to-valley difference in height values (Z range). All parameters were analyzed with the WinSPM software [68].

The crystal structure of the $LaTiO_3$ compound was studied by TEM with a JEM-1200EXII Jeol microscope. The diffraction patterns were taken with a voltage of 120 kV and a current intensity of 70–80A, with camera length of 100 cm. The specimens were prepared by dispersing small amounts of powders of the $LaTiO_3$ nanocrystals by ultrasonification at ultrasonic power of 40% during 35 min in toluene (Sigma-Aldrich, 99.8%).

3. Results and Discussion

3.1. Structural Characterization

Fig. 3 shows the thermal behavior of the gel from 25 °C up to 1100 °C. The analysis of the DTA curve is divided in three regions: 25–200 °C, 200–600 °C and 600–1000 °C. In the first region there is the loss of water up to 150 °C. In the next region the loss of weight continues due to the break-up of EDTA compounds into carbonates and nitrates and the decomposition of the residual organics. The region between 400 °C and 600 °C is associated with the decomposition of most of the organic part and release of N_xO_y, O_2, CO and CO_2 gasses [69]. After 600 °C a decrease in the curve means the complete denaturalization of the organic part and the reaction of NO_x group with residuals of the organic part at 248 °C, which is in agreement with the results of Liu C.-E. et al. [69].

In the last region, up to 1000 °C of two exothermic peaks are observed at 675 and 686 °C. They are probably due to the initial formation of monoclinic perovskite $La_2Ti_2O_7$ (space group $P2_1$) compound taking place. After 700 °C the complete formation of the $La_2Ti_2O_7$ compound is achieved and it represents the thermal stability of nanosized metastable

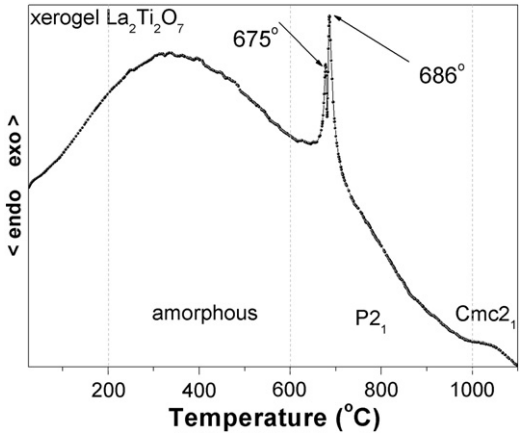

Fig. 3 – Differential thermal curve for La–Ti gel precursor to identify the formation of $La_2Ti_2O_7$ compound.

monoclinic $La_2Ti_2O_7$ due to the small size effects. The XRD patterns of $La_2Ti_2O_7$ support the thermo analysis results as one can read in the next section.

The thermal decomposition behavior of the obtained La–Ti–sol–gel precursor was investigated by TG-DSC method and the results are shown in Fig. 4. The TG curve (solid line) demonstrates three continuous weight-loss regions in the range of 25–250 °C (about 7%), 250–450 °C (about 37%) and 400–650 °C (about 15%) respectively. The first weight-loss corresponds to the elimination of physically adsorbed water. The second weight-loss region can be ascribed to the pyrolysis of NO_3^-, some organic phases and decomposition of H_2SO_4 acid. The third weight loss is associated to the elimination of the remaining organic materials (carbon and organic compounds) and the formation of monoclinic perovskite $La_2Ti_2O_7$ phase with special group $P2_1$. The DSC curve (dots) shows four features. The endothermic process in the region of 70–250 °C is believed to be from the removal of the adsorbed water [69,70]. The endothermic and exothermic peaks in the region of 350–450 °C are attributed to the decomposition of the organic phase [69,70]. The exothermic peak around 653 °C is

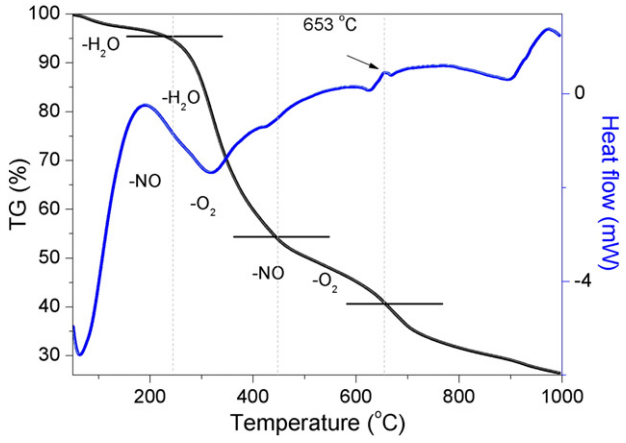

Fig. 4 – Thermo gravimetric and differential scanning curves for the La–Ti–gel precursor to corroborate the differential thermal results.

due to the burning out of the residual organics as well as the crystallization of $La_2Ti_2O_7$ inorganic phase, which is consistent with the TG analysis.

XRD patterns of $La_2Ti_2O_7$ powders prepared by the sol–gel acrylamide route under different temperatures are shown in Fig. 5 within the 2θ range of 20° to 70°. These steps were important to determine the optimum heat treatment to obtain the $La_2Ti_2O_7$ compound.

Panel (a) of Fig. 5 shows the reflections from the standard XRD card (JCPDS No. 81-1066). Fig. 5b shows the sample derived from the heat treatment at 100 °C during 12 h. At this stage it only contains the peaks attributed to La_2O_3 and $La(OH)_3$. There is no significant reflection peak due to $La_2Ti_2O_7$ and TiO_2, which demonstrate that the dominating phase of the powders is still amorphous. Panel (c) shows the XRD pattern for the product derived from the thermal treatment at 600 °C during 12 h. It shows weaker intensities and broader diffraction peaks. Both are indicative of a very fine grain size. At this stage the XRD reflections start to show agreement with the monoclinic perovskite $La_2Ti_2O_7$ crystal phase with spatial group $P2_1$. Fig. 5d shows clearly that all diffraction lines match well with the characteristic reflections of $La_2Ti_2O_7$ crystalline phase according to the JCPDS 81-1066. Thus monoclinic layered-perovskite $La_2Ti_2O_7$ with $P2_1$ space group [6,71] is presented in our sample. The lattice parameters of $La_2Ti_2O_7$ heated at 800 °C during 12 h are: a = 7.8081(3) Å, b = 13.0171(6) Å c = 5.5468(1) Å, and β = 98.516°; the reliability parameters for the Rietveld refinements were: Rp (%) = 9.30, Rwp (%) = 10.56 with χ^2 = 1.38.

Panel (e) shows the diffraction pattern obtained after heating to 1000 °C during 3 h. The peak intensity becomes much stronger and the full-width at half maximum (FWHM) becomes narrower, but no diffraction peaks belonging to a secondary phase are found. This XRD result reveals that particle size increases and also indicates that the nanopowders crystallize very well. At this stage, $La_2Ti_2O_7$ with the monoclinic space group $P2_1$ transforms its structure into one with the orthorhombic space group $Cmc2_1$ which is in agreement with the results of N. Ishizawa et al. [6].

This orthorhombic structure has been determined from the refinement by Rietveld method with the lattice parameters reported by N. Ishizawa et al., [6] and J. López-Pérez J. Iñiguez [72]. Table 1 displays the unit cell parameters of orthorhombic perovskite $La_2Ti_2O_7$ crystalline phase derived from the Rietveld refinement using all the observed reflections. The Rp and Rwp reliability parameters for the Rietveld refinements were 19.72% and 15.24% respectively with χ^2 = 1.40.

One can observe that the full width at half maximum value of the peaks decreases as the temperature increases. An estimate of the particle sizes of the powders heated at 600 and 800 °C during 12 h from the Scherrer's equation on the half width of XRD peaks gives crystal size distributions centered on 30.89 and 55.4 nm, respectively.

Fig. 5f shows the reflections from the standard XRD card (JCPDS No. 82-1434). Panel (g) of Fig. 5 shows the XRD pattern for $LaTiO_3$ compound obtained by heating at 850 °C during 5 days and then quenching in ice. Table 2 displays the unit cell parameters of orthorhombic perovskite $LaTiO_3$ crystalline phase derived from the Rietveld refinement using all the observed reflections. The Rp and Rwp reliability parameters

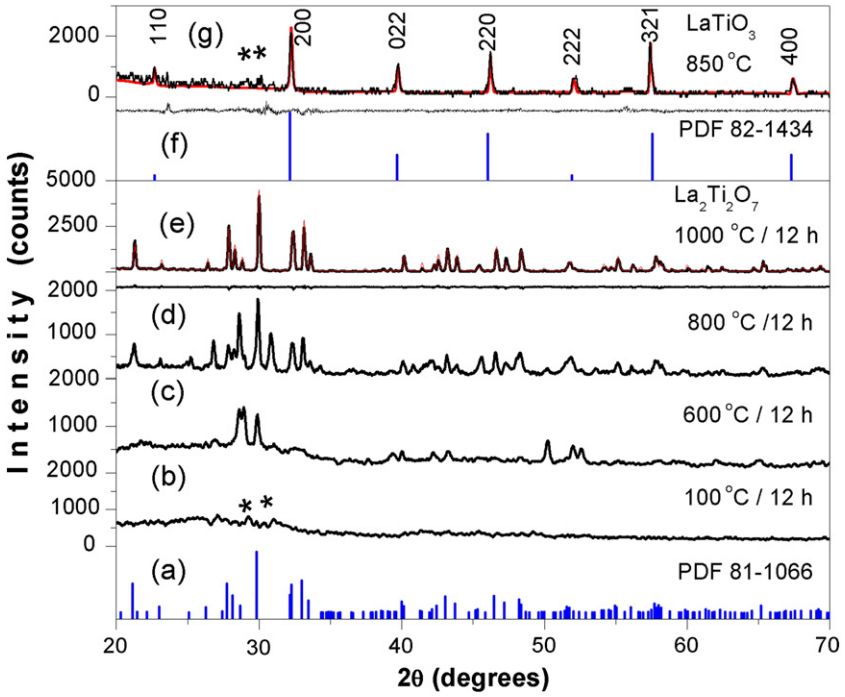

Fig. 5 – (a) Standard XRD card (JCPDS No. 81-1066). XRD patterns of $La_2Ti_2O_7$ prepared by SGAP at (b) 100 °C during 12 h, [*, La_2O_3], (c) 600 °C during 12 h, (d) 800 °C during 12 h, and (e) 1000 °C during 12 h. (f) Standard XRD card (JCPDS No. 82-1434). (g) XRD patterns of $LaTiO_3$ obtained by quenching in ice after 850 °C during 5 days.

for the Rietveld refinements were 8.82% and 9.25% respectively with $\chi^2 = 1.35$. The Rp and Rwp reliability parameters for the Rietveld refinements of tetragonal doped-zirconias indicate that the structural model proposed for these samples fits the experimental results.

3.2. *Microstructural Characterization*

As inferred from the DTA and XRD results the whole process of $LaTiO_3$ formation from annealed La–Ti gel precursors at different temperatures occurs through three steps. The monoclinic perovskite $La_2Ti_2O_7$ with space group $P2_1$ formed at the crystallization beginning from gels; its transformation into one with orthorhombic space group $Cmc2_1$ and the final orthorhombic $LaTiO_3$ phase. In order to obtain a more complete picture of the reactivity from the La–Ti gel precursors to the $LaTiO_3$ phases, it is worthwhile to relate the structural changes to the microstructural transformations. Thus, the microstructural evolution of samples $La_2Ti_2O_7$ and $LaTiO_3$, were examined by scanning electron microscopy (SEM), atomic force microscopy (AFM) and transmission electron microscopy (TEM).

Fig. 6 shows the evolution of the SEM micrographs from the La–Ti gel precursor obtained at 600 °C up to the transformation of $LaTiO_3$ compound. Fig. 6a shows the morphology of the sample obtained after the heat treatment at 600 °C during 12 h. The image reveals rectangular-like grains formed of aggregations of different flaky-like particles. The rectangular-like grains show irregular shapes with the length and width in the nanometer scale ~30–50 nm. The flaky particles are present in non-homogeneous size distribution. However, one can observe

Table 1 – Crystallographic data and results of Rietveld refinement of X-ray powders diffraction patterns of the orthorhombic perovskite $La_2Ti_2O_7$ heated at 1000 °C for 12 h.

$Cmc2_1$	a = 3.9044(3) Å	b = 25.7213(3) Å	c = 5.5440(1) Å	α = β = γ = 90°
Atom	Wyc.	x	y	z
La(1)	4a	0	0.2978(3)	0.1669(1)
La(2)	4a	0	0.4464(5)	0.7515(3)
Ti(1)	4a	1/2	0.3369(2)	0.7069(1)
Ti(2)	4a	1/2	0.4407(7)	0.2422(7)
O(1)	4a	1/2	0.2803(8)	0.9216(5)
O(2)	4a	1/2	0.2960(1)	0.4399(1)
O(3)	4a	1/2	0.3843(4)	0.0415(6)
O(4)	4a	1/2	0.4072(8)	0.5554(4)
O(5)	4a	1/2	0.4901(5)	0.9724(8)
O(6)	4a	0	0.3460(1)	0.7421(8)
O(7)	4a	0	0.4507(6)	0.2609(3)

Table 2 – Crystallographic data and results of Rietveld refinement of X-ray powders diffraction patterns of the orthorhombic perovskite $LaTiO_3$ heated at 850 °C for 5 days.

Pbnm	a = 5.6292(2) Å	b = 5.6121(1) Å	c = 7.9151(1) Å	α = β = γ = 90
Atom	Wyc.	x	y	z
La	4c	0.9920(4)	0.0366(1)	0.25
Ti	4b	0	0.5	0
O(1)	4c	0.0731(7)	0.4884(5)	0.25
O(2)	8d	0.7110(8)	0.2907(3)	0.040(5)

in the micrograph obtained after heating to 800 °C during 12 h (Fig. 6b), the very thin flaky morphologies with a homogenous crystallite size and shape distribution. This result is typical of layered types of structures where the stacked perovskite layers correspond to the smallest crystal dimension. A distribution of flaky particle sizes was observed, with the lengths and widths of the platelets typically in the range of ~50–70 nm. Global EDX results for $La_2Ti_2O_7$ compound prepared by SGAP are presented in the insets of Fig. 6a and b. EDX were taken on the surface of each pellet. One finds higher oxygen concentration at the end of the synthesis in both samples. This is probably due to the oxygen absorption from the atmosphere. The percentage concentrations of cations La and Ti in the $LaTiO_3$ compound determined by this technique are in agreement with those obtained by stoichiometry analysis. This behavior was observed for both samples. The presence of limited amounts of sulfur (0.30%) was detected by this technique, even though it could not be detected by XRD.

Fig. 6c is the micrograph for the powders obtained after the heat treatment at 1000 °C during 12 h. One can observe that the morphology presented in this SEM micrograph shows a grain growth with needle-shape grains. This means that the flaky-shape found in the sample obtained at 600 and 800 °C is maintained throughout the thermal treatments.

Fig. 6d shows the orthorhombic $LaTiO_3$ micrograph on the surface pellet. The pellet was maintained at 850 °C during 5 days in vacuum using a metallic Ti rod as gatherer. One can observe quasi-spherical particle aggregates with a bimodal

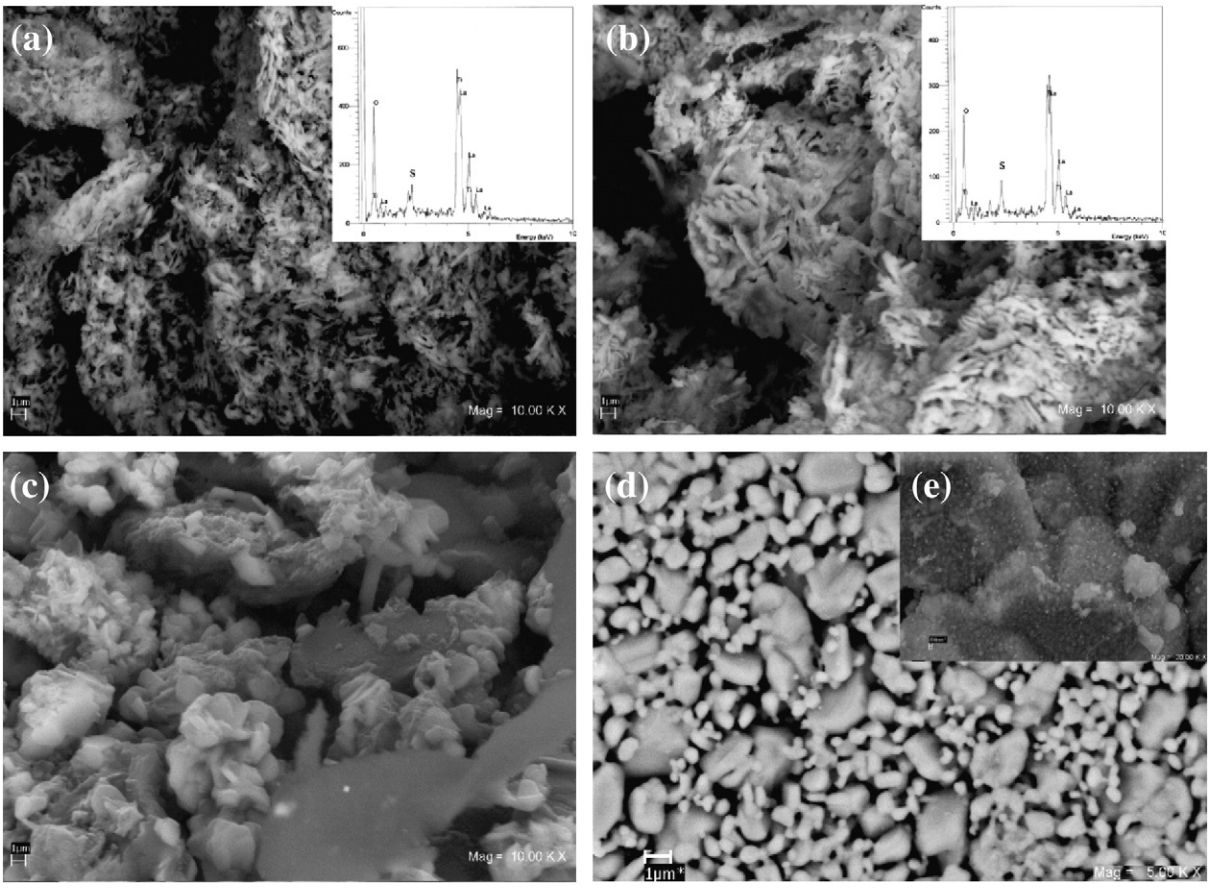

Fig. 6 – (a) SEM microstructure of powders obtained at 600 °C during 12 h. (b) SEM micrograph for powders obtained at 800 °C during 12 h with monoclinic $La_2Ti_2O_7$ crystal structure. (c) SEM micrograph for powders obtained at 1000 °C during 12 h with orthorhombic $La_2Ti_2O_7$ crystal structure. (d) Rounded morphology obtained after reduction with Ti to obtain the orthorhombic $LaTiO_3$ crystal structure.

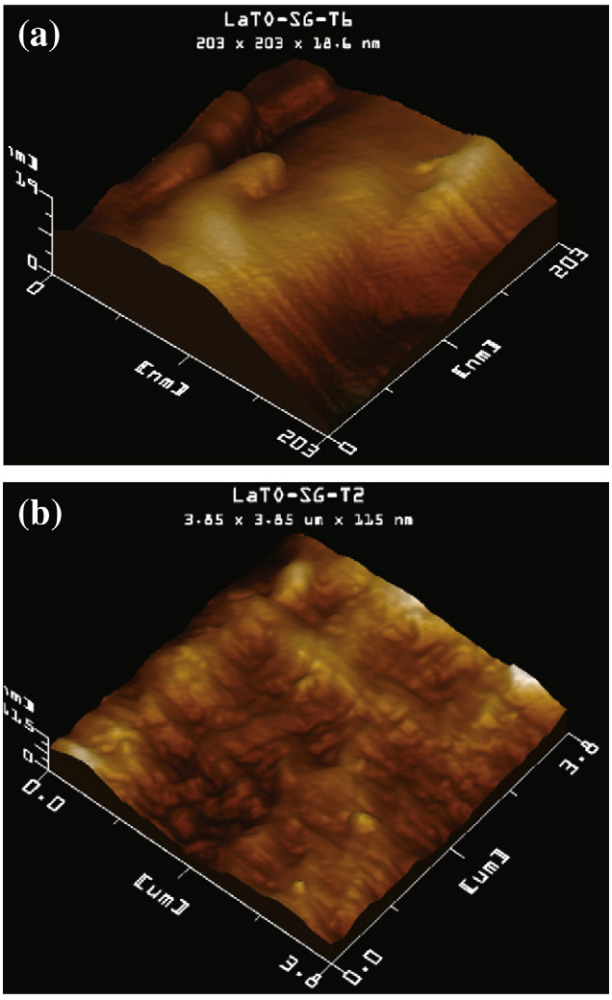

Fig. 7 – (a) AFM micrograph obtained by AC mode of $La_2Ti_2O_7$ powders and (b) AFM micrograph obtained by AC mode of $LaTiO_3$ powders. The images were performed with clock speed of 666.70 μs.

grain size distribution with regular rounded shape. The two average grain sizes are centered at 505 nm and 2 μm. The inset (Fig. 5e) shows the magnification of these quasi-spherical particle aggregates. A narrow, bimodal size and shape distribution in the range between 100 and 250 nm was found for this particles. In any case, the powders obtained from the reduction of the precursor (Fig. 6b) experienced significant grain growth, perhaps secondary recrystallization, resulting in well-defined grains with more rounded grains. These nanoparticles were dissolved by ultrasonification as one can observe in the TEM section.

In order to corroborate the morphology evolution of $La_2Ti_2O_7$ to $LaTiO_3$ compounds we evaluate the surface topography modifications by AFM. Fig. 7a shows the AFM image of the surface of the $La_2Ti_2O_7$ obtained at 600 °C during 12 h. This result confirms the flaky morphology observed by SEM. One can observe that the roughness, determined on a 203 nm × 203 nm surface, is 19 nm. Fig. 7b shows the AFM image for $LaTiO_3$ powders, the image reveals a granular morphology. The well-rounded grains exhibiting a bimodal distribution in size in the range of 0.4–2.5 μm. The roughness determined on a 3.8 μm × 3.8 μm surface is 115 nm.

The TEM image of $LaTiO_3$ compound (Fig. 8a) showed that the aggregation among the particles still remains after ultrasonification. It can be seen from the figure that the particles are polyhedral in shape with strong particle agglomeration and wide size distribution. In this figure one can observe also, the corresponding selected area electron diffraction (SAED) pattern of the sample. There are distinct rings indicating characteristic of nanocrystallites. Five micrographs were analyzed using Image J software [73] in order to obtain the average value of around 36.71 ± 1.78 nm (Fig. 8b).

4. Conclusions

The amorphous La_2O_3–TiO_2 powders were prepared by sol–gel acrylamide polymerization route.

The crystallization pathway on heat treated amorphous La_2O_3–TiO_2 powders were followed by X-ray diffraction (XRD) and the microstructural changes by scanning, transmission electron microscopy and atomic force microscopy (SEM, TEM and AFM, respectively).

XRD results indicated the formation of monoclinic perovskite $La_2Ti_2O_7$ nanocrystals with space group $P2_1$ as a

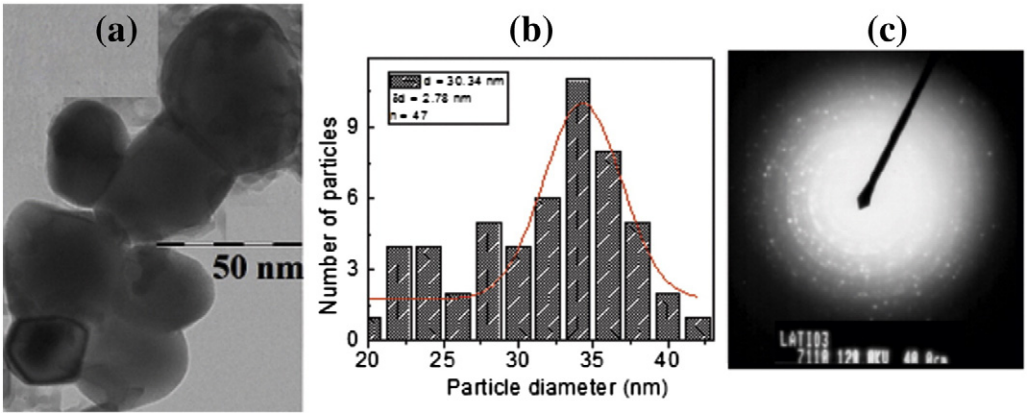

Fig. 8 – (a) Transmission electron micrograph. (b) A particle-size histogram measured from the TEM image in (a). (c) The corresponding selected area diffraction pattern of the orthorhombic $LaTiO_3$.

first step on the whole process to the final orthorhombic $LaTiO_3$ compound.

The microstructural examination of specimens after a heat treatment at 600 °C during 12 h revealed the development of flaky monoclinic perovskite $La_2Ti_2O_7$ nanoparticles with sizes around 30–50 nm. This is to be compared with the samples after a heat treated at 1000 °C during 12 h that show orthorhombic perovskite $La_2Ti_20_7$ (space group $Cmc2_1$) nanocomposites with sizes around 2–4 μm.

The formation of the final orthorhombic perovskite $LaTiO_3$ nanocrystals heated at 850 °C during 5 days, occurred by the quenching in ice. The microstructural examination of $LaTiO_3$ powders reveals a granular morphology. The well-rounded grains exhibit a bimodal distribution in size in the range of 0.4–2.5 μm.

Acknowledgments

G. Herrera thanks Mexico-CONACyT for the student fellowship Grant No. 170588; Posdoctoral Research Scholarship No. 129569 and No. 172529. G. Herrera would like to thank especially MSc. L. Baños, MSc. A. Tejeda-Cruz, Dr. J. Guzmán and C. Flores for their assistance in XRD, SEM, AFM and TEM characterizations at the Instituto de Investigaciones en Materiales UNAM. G. H. wants to thank to A. Moreno for the library facilities at PUEC-UNAM. J. Jiménez-Mier acknowledges support from grants UNAM-PAPIIT IN109308, CONACyT U41007-F and 56764.

REFERENCES

[1] Yang Y, Sun YB, Jiang YS. Structure and photocatalytic property of perovskite and perovskite-related compounds. Mater Chem Phys 2006;96:234–9.
[2] Aurivillius B. Mixed bismuth oxides with layer lattices. Ark Kem 1949;1:463–70.
[3] Fuierer PA, Newnham RE. $La_2Ti_2O_7$ ceramics. J Am Ceram Soc 1991;74:2876–81.
[4] Zhang FX, Lian J, Becker U, Ewing RC, Wang LM, Hu J, et al. Structural change of layered perovskite $La_2Ti_2O_7$ at high pressures. J Solid State Chem 2007;180:571–6.
[5] Ishizawa N, Marumo F, Iwai S, Kimura M, Kawamura T. Compounds with perovskite-type slabs. III. The structure of a monoclinic modification of $Ca_2Nb_2O_7$. Acta Crystallogr B 1980;36:763–6.
[6] Ishizawa N, Marumo F, Iwai S, Kimura M, Kawamura T. Compounds with perovskite-type slabs. V. A high-temperature modification of $La_2Ti_2O_7$. Acta Crystallogr B 1982;38:368–72.
[7] Brandon JK, Megaw HD. On the crystal structure and properties of $Ca_2Nb_2O_7$. Philos Mag 1969;21:189–94.
[8] Venet M, Vendramini A, Santos IA, Eiras JA, Garcia D. Texturing and properties in hot forged SBN63/37 ceramics. Mater Sci Eng B 2005;117:254–60.
[9] Subramanian MA, Aravamundan G, Subba Rao GV. Oxide pyrochlores — a review. Prog Solid State Chem 1983;15:55–143.
[10] Shannon RD. Revised effective ionic radii and systematic studies of interatomic distances in halides and chalcogenides. Acta Crystallogr A 1976;32:751–67.
[11] Nanamatsu S, Kimura M, Doi K, Matsushita S, Yamada N. A new ferroelectric: $La_2Ti_2O_7$. Ferroelectrics 1974;8:511–3.
[12] Shcherbakova LG, Mamsurova LG, Sukhanova GE. Rare earth element titanates. Usp Khim 1979;48:423–47.
[13] Takahashi J, Otsuka T. Vibrational spectroscopic study of structural evolution in the coprecipitated precursors to lanthanum tin oxide $La_2Sn_2O_7$ and lanthanum titanium oxide $La_2Ti_2O_7$. J Am Ceram Soc 1989;72:426–31.
[14] Suresh M, Prasadarao AV, Komarneni S. Mixed hydroxide precursors for $La_2Ti_2O_7$ and $Nd_2Ti_2O_7$ by homogeneous precipitation. J Electroceram 2001;6:147–51.
[15] Li K, Wang Y, Wang H, Zhu M, Yan H. Hydrothermal synthesis and photocatalytic properties of layered $La_2Ti_2O_7$ nanosheets. Nanotechnology 2006;17:4863–7.
[16] Song H, Peng T, Cai P, Yi H, Yan C. Hydrothermal synthesis of flaky crystallized $La_2Ti_2O_7$ for producing hydrogen from photocatalytic water splitting. Catal Lett 2007;113:54–8.
[17] Kim J, Hwang DW, Bae SW, Kim YG, Lee JS. Effect of precursors on the morphology and the photocatalytic water-splitting activity of layered perovskite $La_2Ti_2O_7$. Korean J Chem Eng 2001;18:941–7.
[18] Kim HG, Hwang DW, Bae SW, Jung JH, Lee JS. Photocatalytic water splitting over $La_2Ti_2O_7$ synthesized by the polymerizable complex method. Catal Lett 2003;91:193–8.
[19] Shcherbakova LG, Mamsurova LG, Sukhanova GE. Lanthanide titanates. Russ Chem Rev 1979;48:228.
[20] Balachandran U, Eror NG. X-ray diffraction and vibrational-spectroscopy study of the structure of $La_2Ti_2O_7$. J Mater Res 1989;4:1525–8.
[21] Seo JW, Fompeyrine J, Locquet JP. Microstructural investigation of $La_2Ti_2O_7$ thin films grown by MBE, Superconducting and related oxides. Phys Nanoeng III 1998;326:3481.
[22] Fompeyrine J, Seo JW, Locquet JP. Growth and characterization of ferro-electric $LaTiO_{3.5}$ thin films. J Eur Ceram Soc 1999;19:1493–6.
[23] Kushkov D, Zverlin AV, Zaslavskii AM, Slivinskaya AE, Melnikov AV. Structure of the $Ln_2Ti_2O_7$ thin films prepared by pulsed laser deposition. J Mater Sci 1993;28:361–3.
[24] Havelia S, Balasumramaniam KR, Spurgeon S, Cormack F, Salvador PA. Growth of $La_2Ti_2O_7$ and $LaTiO_3$ thin films using pulsed laser deposition. J Cryst Growth 2008;310:1985–90.
[25] Yamamoto JK, Bhalla AS. Piezoelectric properties of layered perovskite $A_2Ti_2O_7$ (A = La and Nd) single-crystal fibers. J Appl Phys 1991;70:4469–71.
[26] Prasadaro AV, Selvaraj U, Komarneni S, Bhalla AS. Sol–gel synthesis of Ln_2 (Ln = La, Nd)Ti_2O_7. J Mater Res 1992;7:2859–63.
[27] Prasadaro AV, Selvaraj U, Komarneni S, Bhalla AS. Fabrication of $La_2Ti_2O_7$ thin films by a sol–gel technique. Ferroelectr Lett 1992;14:65–72.
[28] Prasadaro AV, Selvaraj U, Komarneni S, Bhalla AS. Grain orientation in sol–gel derived $Ln_2Ti_2O_7$ ceramics (Ln = La, Nd). Mater Lett 1991;12:306–10.
[29] Milanova MM, Kakihana M, Arima M, Yashima M, Yoshimura M. A simple solution route to the synthesis of pure $La_2Ti_2O_7$ and $Nd_2Ti_2O_7$ at 700–800 °C by polymerized complex method. J Alloys Compd 1996;242:6–10.
[30] Pechini MP. US Patent 3,330,697, July 11 1967
[31] Wang H, Zuo R, Fu J, Liu Y. Sol–gel derived (Li, Ta, Sb) modified sodium potassium niobate ceramics: processing and piezoelectric properties. J Alloys Compd 2011;509:936–41.
[32] Herrera Pérez G, Chavira E, Jiménez-Mier J, Baños L, Guzmán J, Flores C. Nanostructure obtained by sol–gel acrylamide polymerization in Y–V–O system. Microsc Microanal 2006;12:736–7.
[33] Herrera Pérez G, Chavira E, Jiménez-Mier J, Ordoñez A, Bucio E, Baños L, et al. Direct observation of S–R bonding in nanosized $La_2Ti_2O_7$ and $Y_2Ti_2O_7$ compounds obtained by sol–gel acrylamide polymerization. Microsc Microanal 2007;13:676–7.

[34] Herrera G, Chavira E, Jiménez J, Ordoñez A, Bucio E, Baños L, et al. Microstructural comparison of La–V–O compounds prepared by sol–gel acrylamide polymerization and solid state reaction. Microsc Microanal 2009;15:1044–5.
[35] Herrera G, Chavira E, Jiménez J, Baños L, Guzmán J, Flores C. Synthesis and structural characterization of YVO_3 prepared by sol–gel acrylamide polymerization and solid state reaction methods. J Sol-Gel Sci Technol 2008;46:1–10.
[36] Herrera G, Chavira E, Jiménez J, Ordoñez A, Fregoso E, Baños L, et al. Synthesis and structural characterization of $LaVO_3$ prepared by sol–gel acrylamide polymerization and solid state reaction methods. J Alloys Compd 2009;479:511–9.
[37] Herrera G, Montoya N, Alarcón J. Synthesis and characterization of iron doped $ZrSiO_4$ solid solutions from gels. J Am Ceram Soc 2011;94:4247–55.
[38] Kimura M, Nanamatsu S, Kawamura T, Matsushita S. Ferroelectric, electrooptic and piezoelectric properties of $Nd_2Ti_2O_7$ single crystal. Jpn J Appl Phys 1974;13:1473–4.
[39] Kim WS, Ha SM, Yun S, Park HH. Microstructure and electrical properties of $Ln_2Ti_2O_7$ (Ln = La, Nd). Thin Solid Films 2002;420–421:575–8.
[40] Kim WS, Ha SM, Yang JK, Park HH. Ferroelectric-gate field effect transistors using $Nd_2Ti_2O_7/Y_2O_3$/Si structures. Thin Solid Films 2001;398–399:663–7.
[41] Kimura M, Nanamatsu S, Doe K, Matsushita S, Takahashi M. Electrooptic and piezoelectric properties of $La_2Ti_2O_7$ single crystal. Jpn J Appl Phys 1972;11:904.
[42] Marzullo S, Bunting EN. Dielectric properties of titania or Tin oxide containing varying proportions of rare-earth oxides. J Am Ceram Soc 1958;41:40–1.
[43] Ouchi H, Kawashima S. Proc. 6th Int. Meet. Ferroelectricity. Jpn J Appl Phys, 24; 1985. p. 60.
[44] Fasquelle D, Carru JC, Le Gendre L, Le Paven C. Lanthanum titanate ceramics: electrical characterizations in large temperature and frequency ranges. J Eur Ceram Soc 2005;25:2085–8.
[45] Diallo PT, Boutinaud PB, Mahiou R. Anti-stokes luminescence and site selectivity in $La_2Ti_2O_7:Pr^{3+}$. J Alloys Compd 2002;341:139–43.
[46] Yang HH, Cheng H, Tang YG, Lu ZG. Photoluminescence enhancement of $(La_{0.95}Eu_{0.05})_2Ti_2O_7$ nanophosphors via Li^+ doping. J Am Ceram Soc 2009;92:931–3.
[47] Ikeda S, Hara M, Kondo JN, Domen K. Preparation of $K_2La_2Ti_3O_{10}$ by polymerized complex method and photocatalytic decomposition of water. Chem Mater 1998;10:72–7.
[48] Yang QL, Kang SZ, Chen H, Bu W, Mu J. $La_2Ti_2O_7$: an efficient and stable photocatalyst for the photoreduction of Cr(VI) ions in water. Desalination 2011;266:149–53.
[49] Sulaeman U, Yin S, Sato T. Visible light photocatalytic activity induced by the carboxyl group chemically bonded on the surface of $SrTiO_3$. Appl Catal B 2011;102:286–90.
[50] Hwang DW, Kim HG, Lee JS, Kim J, Li W. Photocatalytic hydrogen production from water over M-doped $La_2Ti_2O_7$ (M = Cr, Fe) under visible light irradiation ($\lambda > 420$ nm). J Phys Chem 2005;109:2093–102.
[51] Hwang DW, Cha KY, Kim J, Kim HG, Hyun G, Bae SW, et al. Photocatalytic degradation of CH_3Cl over a nickel-loaded layered perovskite. Ind Eng Chem Res 2003;42:1184.
[52] Zhao ZT, Zhang YM, Yang J, Li H, Song W, Zhao XQ. Low-temperature synthesis of $La_2Ti_2O_7$ nanocrystal by metallorganic decomposition method. J Ceram Soc Jpn 2005;113:67–70.
[53] Kim J, Hwang DW, Kim HG, Bae SW, Lee JS, Li W, et al. Highly efficient overall water splitting through optimization of preparation and operation conditions of layered perovskite photocatalysts. Top Catal 2005;35:295–303.
[54] Kim HG, Hwang DW, Kim J, Kim YG, Lee JS. Highly donor-doped (110) layered perovskite materials as novel photocatalysts for overall water splitting. Chem Commun 1999:1077–8.
[55] Abe R, Higashi M, Sayama K, Abe Y, Sugihara H. Photocatalytic activity of R_3MO_7 and $R_2Ti_2O_7$ (R = Y, Gd, La; M = Nb, Ta) for water splitting into H_2 and O_2. J Phys Chem B 2006;110:2219–26.
[56] Sunstrom JE, Kauzlarich SM, Klavinst P. Synthesis, structure, and properties of $La_{1-x}Sr_xTi0_3(0 < x < 1)$. Chem Mater 1992;4:346–53.
[57] Cwik M, Lorenz T, Baier J, Muller R, André G, Bourée F, et al. Crystal and magnetic structure of $LaTiO_3$: evidence for non-degenerate t2g-orbitals. Phys Rev B 2003;68:060401.
[58] Kim KH, Norton DP, Budai JD, Chisholm MF, Sales BC, Christen DK, et al. Epitaxial structure and transport in $LaTiO_{3+x}$ films on (001) $SrTiO_3$. Phys Status Solidi A 2003;200:346–51.
[59] Liu BT, Maki K, So Y, Nagarajan V, Ramesh R, Lettieri J, et al. Epitaxial La-doped $SrTiO_3$ on silicon: a conductive template for epitaxial ferroelectrics on silicon. Appl Phys Lett 2002;80:4801.
[60] Hato T, Yoshida A, Yoshida C, Suzuki H, Yokoyama N. Dielectric-base transistors with doped channel. Appl Phys Lett 1997;70:2900.
[61] Li GQ, Lai PT, Zeng SH, Huang MQ, Cheng YC. Photo-, thermal and humidity sensitivity characteristics of $Sr_{1-x}La_xTiO_3$ film on SiO_2/Si substrate. Sens Actuators, A 1997;63:223–6.
[62] Francis S, Varshney L. Studies on radiation synthesis of PVA/EDTA hydrogels. Radiat Phys Chem 2005;74:310–6.
[63] Sin A, Odier P. Gelation by acrylamide, a quasi-universal medium for the synthesis of fine oxide powders for electroceramic applications. Adv Mater 2000;12:649–52.
[64] Universal analysis 2000©version 4405 TA instruments waters LLC; 1998–2006.
[65] Rodriguez-Carvajal J. Abstracts of the meeting powder diffraction, Toulouse France. Chester, UK: International Union of Crystallography; 1990 127.
[66] Rodriguez-Carvajal J. FULLPROF: a program for rietveld refinement and pattern matching analysis. Abstracts of the satellite meeting on powder diffraction of the XV congress of the IUCr. Toulouse, France: International Union of Crystallography; 1990. p. 127.
[67] Rodriguez-Carvajal J, Roisnel T. Commission on powder diffraction, international union of crystallography. Newsletter 1998;20:35.
[68] Leane RB. WinSPM DPS ©version 2.00. JEOL Ltd.; 1989–2002
[69] Liu C-E, Richard-Plouet M, Besland M-P, Albertini D, Estournès C, Brohan L. Dip-coated $La_2Ti_2O_7$ as a buffer layer for growth of $Bi_{3.25}La_{0.75}Ti_3O_{12}$ films with enhanced (0 1 1) orientation. J Eur Ceram Soc 2009;29:1977–85.
[70] Cheng H, Lu Z, Liu Y, Yang H, Gu Y, Li W, et al. Sol-gel synthesis and photoluminescence characterization of $La_2Ti_2O_7:Eu^{3+}$ Nanocrystals. Rare Metals 2011;30:602–6.
[71] Gasperin M. Dititanate de Lanthane. Acta Crystallogr B 1975;31:2129–30.
[72] López-Pérez J, Iñiguez J. Ab initio study of proper topological ferroelectricity in layered perovskite $La_2Ti_2O_7$. Phys Rev B 2011;84:075121.
[73] Rasband W. Image J. Bethesda, Maryland, USA: U. S. National Institutes of Health; 1997–2012. http://imagej.nih.gov/ij/.